Microscopy AND Microanalysis

© MICROSCOPY SOCIETY OF AMERICA 2010

Testate Amoebae Examined by Confocal and Two-Photon Microscopy: Implications for Taxonomy and Ecophysiology

Zuzana Burdíková,[1,2,*] Martin Čapek,[1,3] Pavel Ostašov,[1] Jiří Machač,[4] Radek Pelc,[1] Edward A.D. Mitchell,[5] and Lucie Kubínová[1]

[1]Institute of Physiology, Academy of Sciences of the Czech Republic, v.v.i., Vídeňská 1083, CZ-14220 Prague 4, Czech Republic

[2]Institute of Geology and Paleontology, Faculty of Science, Charles University, Albertov 6, CZ-12843 Prague 2, Czech Republic

[3]Faculty of Biomedical Engineering, Czech Technical University in Prague, nám. Sítná 3105, CZ-27201 Kladno, Czech Republic

[4]Institute of Botany, Academy of Sciences of the Czech Republic, v.v.i., Zámek 1, CZ-25243 Průhonice, Czech Republic

[5]Laboratory of Soil Biology, University of Neuchâtel, Rue Emile-Argand 11, CH-2000 Neuchâtel, Switzerland

Abstract: Testate amoebae (TA) are a group of free-living protozoa, important in ecology and paleoecology. Testate amoebae taxonomy is mainly based on the morphological features of the shell, as examined by means of light microscopy or (environmental) scanning electron microscopy (SEM/ESEM). We explored the potential applications of confocal laser scanning microscopy (CLSM), two photon excitation microscopy (TPEM), phase contrast, differential interference contrast (DIC Nomarski), and polarization microscopy to visualize TA shells and inner structures of living cells, which is not possible by SEM or environmental SEM. Images captured by CLSM and TPEM were utilized to create three-dimensional (3D) visualizations and to evaluate biovolume inside the shell by stereological methods, to assess the function of TA in ecosystems. This approach broadens the understanding of TA cell and shell morphology, and inner structures including organelles and endosymbionts, with potential implications in taxonomy and ecophysiology.

Key words: testate amoebae, confocal microscopy, environmental scanning electron microscopy, taxonomy, ecophysiology

INTRODUCTION

Testate amoebae (TA) belong to a polyphyletic group of unicellular eucaryotes (ca. 10–400 μm) protected by a shell (test). The shell enclosing the cell plasma usually has a single aperture (operculum) for the pseudopodia, rarely two apertures. A proteinaceous organic matrix is the basic shell component (Meisterfeld, 2002a, 2002b). There are four main shell types: proteinaceous only, calcareous, siliceous (species secreting their own regular siliceous shell plates, so-called idiosomes), and agglutinated (species incorporating extraneous mineral particles, so-called xenosomes, into their shells) (Wanner, 1999). Despite the presence of an opaque shell, some testate amoeba species have photosynthetic endosymbionts and are thus mixotrophic (Meisterfeld, 2002a, 2002b).

Testate amoebae are commonly used as model organisms in population ecology, ecotoxicology, ecology, paleoecology, and evolutionary biology. They are useful bioindicators of natural ecological gradients, environmental stress, or pollution in both aquatic and terrestrial ecosystems (Patterson et al., 1996, 2002; Foissner, 1997, 1999; Booth, 2002; Mitchell et al., 2008a, 2008b). In most aquatic and terrestrial ecosystems, TA also play an important role in the cycling of nutrients, especially C, N, and Si (Schönborn, 1983, 1992; Schröter et al., 2003; Aoki et al., 2007; Wilkinson, 2008; Vohník et al., 2009).

A prerequisite for the use of TA in ecological and paleoecological studies is a sound taxonomy. TA taxonomy is mainly based on the shell structure (Ogden & Hedley, 1980). Indeed, in a number of taxa the cytoplasm, the nuclei and types of pseudopodia have not been observed yet (Meisterfeld, 2002a, 2002b). Recent studies combining morphological and molecular data have revealed an unexpected diversity among the testate amoebae, thus illustrating their role as a model group to study evolutionary processes such

as marine-terrestrial transitions. Subtle morphological features that are typically invisible under light microscopy were shown be of taxonomical significance (Todorov et al., 2009; Heger et al., 2010).

Ecological studies aiming to establish the contribution of TA to biomass or nutrient cycling require a reliable estimate of cell volume (e.g., Gilbert et al., 1998; Mitchell et al., 2003; Schröter et al., 2003). The volume of biomass inside the shells can be calculated by applying an appropriate conversion factor (Madrid & Felice, 2005) or by assuming that the TA shells can be approximated by simple geometrical shapes (Gilbert et al., 1998). The accuracy of these approaches is limited (Charrière et al., 2006).

There has been a growing demand to revise the taxonomy of testate amoebae and to develop new optical methods for their reliable identification (Mitchell & Gilbert, 2010). Apart from scanning electron microscopy (SEM) as the most common technique, the ideal imaging setup should distinguish the relevant morphological features without requiring an excessively complex preparation and handling. To some extent, the optical contrasting modalities such as phase contrast, differential interference contrast (DIC) (Murphy, 2001) or digital holographic microscopy, a modern adaptation of interference microscopy (Charrière et al., 2006) can be utilized, as demonstrated in TA (Beyens & Meisterfeld, 2001; Charrière et al., 2006). If biovolume estimations and/or three-dimensional (3D) reconstructions are required confocal or two-photon microscopy represent a convenient solution.

The aim of the present study is to explore the potential of confocal laser scanning microscopy (CLSM) and two-photon excitation microscopy (TPEM) together with 3D reconstructions and stereological measurements for the study of testate amoebae morphology.

MATERIALS AND METHODS

Specimens

Samples of TA were collected from four pools of Komořany ponds near Vltava river, 1–2 m from the river, in Prague, Czech Republic. TA from Komořany pools were studied without fixation and stored in their natural environment (water) for not more than 4 h before image acquisition. Samples from the Alps and Jura Mountains (Switzerland) and from *Sphagnum* moss areas of the Šumava Mountains (Czech Republic) were studied both before and after a paraformaldehyde fixation. A list of all examined species is shown in Table 1.

The fixation was performed by a gentle centrifugation followed by replacing the resulting supernatant by 4% paraformaldehyde (45 min at room temperature). After fixation the specimen was centrifuged again and supernatant replaced by filtered water (0.2 μm mesh) obtained from the place of sampling.

For DAPI, Hoechst 34580, propidium iodide, and Alexa-Fluor 633 phalloidin staining, the TA were fixed and treated

with 0.1% Triton X-100 (5 min at room temperature) to permeabilize the plasma membrane. The samples were then centrifuged, Triton X-100 aspired, and the samples suspended in water. Triton X-100 was not used when identifying dead/living cells by propidium iodide staining (Table 1, Fig. 3h).

The TA samples were stained as specified in Table 2, centrifuged in Eppendorf tubes (12,100 rpm for 45 s, RCF ca. 9,000 g), supernatant removed and replaced with filtered water (0.2 μm mesh) from the place of sampling. The centrifugation was performed three times to remove any excessive probe. Afterwards, the TA suspension in water was mounted between a microscope slide and a cover slip sealed together with nail varnish.

Optical Contrasting

All images shown in Figure 1 were acquired with an Olympus DP70 digital camera fitted to an Olympus BX60 upright microscope equipped with U-UCD8 universal condenser (NA 0.90 in a dry "TLD" mode).

Conventional phase contrast with no special modifications was employed. Polarization microscopy was performed in a simple way, with the specimen placed between crossed or nearly crossed polarizers. Differential interference contrast (DIC Nomarski) images were optimized by adjusting the position of the Wollaston prism in a DIC slider (U-DICT type), thus setting an optimal bias retardation, depending on the optical thickness of the object (testate amoeba). Two objective lenses were used: UPlanFl 40x/0.75 Ph2 (Fig. 1b) and UPlanFl 20x/0.50 (all other images).

Except for Figures 1f,h, all images shown in Figure 1 are processed ones obtained from raw images acquired at a series of focal planes, by employing a DeepFocus module of QuickPHOTO Micro software.

Scanning and Environmental Scanning Electron Microscopy

A scanning electron microscope FEI Quanta 200 was used as described in (Michels & Schnack-Schiel, 2005), either in SEM or environmental SEM (ESEM) mode.

For the SEM (high-vacuum) mode, the fixed shells were critical point dried or partially dried, mounted on metal stubs with a double-sided adhesive conductive (carbon) tape and coated with gold (4 min at 20 mA in a vacuum of about 10 Pa, with argon present) using a sputter coater. The stubs were then affixed by the carbon tape to a microscope stage. The gold-coated TA shells were examined at 20–30 kV in a high vacuum mode, using an Everhart-Thornley secondary electron detector.

For the ESEM mode, the fixed shells were washed in distilled water to remove the fixatives, partially dried, and placed on a Peltier-cooled stage (JT Manufacturing, Hudson, NH, USA). To prevent the stub from drifting, it was previously covered with the same double-sided adhesive conductive (carbon) tape as used in SEM. The TA shells were observed at 20–30 kV, 200–400 Pa, and sample temper-

Table 1. A List of Observed Testate Amoebae Species and Tested Fluorescent Probes.[*]

Species	Probe/Number of Examined TA	Number of All/Living Cells (P and B Probes Combined)
Arcella vulgaris Ehrenberg *Arcella discoides* Ehrenberg	A/3, B/2, C/3, D/1, M/2, P/5, TR/2	55/7
Archerella flavum (Archer)	A/3	
Assulina muscorum Greeff *Assulina seminulum* Penard	A/10, B/10, D/10, DI/10, F/10, PH/10, S/1	
Centropyxis aculeata (Ehrenberg) Stein *Centropyxis aerophila* Deflandre *Centropyxis constricta* (Ehrenberg) Penard	A/5, AB/3, B/45, D/7, P/6, T/5, TR/8	66/18
Corythion dubium Taranek	B/1	
Cyclopyxis eurystoma Deflandre *Cyclopyxis kahli* Deflandre	B/4, T/7	
Cyphoderia ampulla Ehrenberg		1/1
Difflugia oblonga Ehrenberg	B/3, D/4, H/3, P/3, T/8	21/4
Euglypha ciliata Ehrenberg *Euglypha compressa* Carter *Euglypha strigosa* Ehrenberg	B/5, C/3, D/2, E/5, H/2, L/5, M/10, P/6, S/1, T/3	31/10
Hyalosphenia papilio Leidy	A/10, B/10, D/10, DI/10, F/10, PH/10, S/3, T/4	
Nebela bohemica Taranek *Nebela tincta* Leidy	A/10, B/10, C/3, D/10, DI/10, F/10, PH/10	
Tracheleuglypha dentata Penard	A/3, B/5, D/4, P/3, T/6	21/5
Trinema complanatum Penard *Trinema enchelys* Ehrenberg *Trinema lineare* Penard	A/10, B/28, D/11, H/3, P/6, T/20, TR/6	68/8
Trigonopyxis arcula Penard	AB/4	

[*]The following notation was used: A (Acid Fuchsin), AB (Aniline Blue), B (BCECF-AM), C (CellTracker Green CMFDA), D (DAPI), DI (DiOC$_3$(3)), E (Er-Tracker Blue-White DPX), F (FITC), H (Hoechst 34580), L (LysoTracker Red DND-99), M (MitoTracker Deep Red FM), P (propidium iodide), PH (AlexaFluor 633 phalloidin), S (SYTO 16), T (TMRE), TR (Texas Red C$_2$-maleimide). The third column indicates the number of all individuals in a combined propidium iodide and BCECF-AM staining experiment (before slash) and the number of individuals identified as alive by this method (after slash).

ature of −14°C to −4°C. Alternatively, the pressure was raised up to 1 kPa with no cooling applied. A gaseous secondary electron detector was used.

Confocal Laser Scanning Microscopy

Two confocal laser scanning microscope systems were used: (1) Leica TCS SPE based on Leica DM 2500 CSQ V-VIS fluorescence microscope and equipped with four solid state lasers, 405 nm (25 mW), 488 nm (15 mW), 532 nm (15 mW), 635 nm (15 mW); (2) Leica TCS SP2 AOBS based on Leica DM IRE2 inverted microscope and equipped with continuous lasers; Ar: 458 nm (5 mW), 476 nm (5 mW), 488 (20 mW), 514 nm (20 mW); HeNe: 543 nm (1.2 mW), 633 nm (10 mW).

The laser power and detector offset and gain were manually adjusted prior to image stack collection, so that the best combination of black background and avoidance of black pixels and oversaturation in the structures of interest was achieved. The image stacks were obtained by collecting optical sections throughout the entire thickness of the specimen. The images (optical sections) were acquired using scan rates and frame averaging settings to yield the best signal-to-noise ratio within a reasonable collection time. In most cases water immersion planapochromat objectives HC PL APO 20x/0.70 IMM CORR CS and HCX PL APO 63x/1.20 W CORR CS were used.

Due to attenuation of the light arising from deeper parts of the sample, the images in the acquired stack were enhanced by two methods: (1) online method—an intensity compensation feature of Leica Confocal Software (version 2.61, Leica Microsystems GmbH, Heidelberg, Germany) in a "linear-by-gain" mode, adjusting the photomultiplier tube gain according to the z-coordinate of the current image and

Table 2.   Excitation and Emission Wavelengths, Staining Protocols, and Targets of Applied Fluorescent Probes.

Fluorescent Probe[*1]	Excitation/Detection Wavelength[*2] (nm)	Final Concentration	Staining Time (min)	Targets[*3]
Acid Fuchsin (84600)	543/600–650	170 μM	10	Chitin, vacuoles, cytoplasm
AlexaFluor 633 phalloidin (A22284)	633/650–700	130 nM	120	Actin
Aniline Blue (ANIL01600)	405/500–550	135 μM	10	Chitin
BCECF–AM (B8806)	458 and 488/500–550	2 μM	25	Cytoplasm, pH
CellTracker Green CMFDA (C7025)	488/500–580	4 μM	30	Cytoplasm, only metabolically active cells
DAPI (D1306)	405/450–520	300 μM	20	Nucleic acids
DiOC$_3$(3) (43580)	488(1P), 950 (2P)/500–650[*4]	13.6 μM, 4.5 μM	20–25	Membranes
Er-Tracker Blue-White DPX (E12353)	405 (1P), 790 (2P)/430–640[*4]	2 μM	120	Endoplasmic reticulum
FITC (46952)	488 (1P), 950 (2P)/500–580[*4]	1 mM	20	General staining, aminogroups
Hoechst 34580 (H21486)	405/430–490	1.8 mM	30	Nucleic acids
LysoTracker Red DND-99 (L7528)	543/580–620	200 nM	120	Lysosomes
MitoTracker Deep Red FM (M22426)	633/640–650	1 μM	120	Mitochondria
Propidium Iodide (70335)	532/600–670	7.5 μM	25	Nucleic acids
SYTO 16 (S7578)	488/500–530	10 μM	90	Nucleic acids
Texas Red C$_2$-maleimide (T6008)	532/600–650	14 nM	40	General staining
TMRE (T669)	532/560–590	1 μM	20	Mitochondria

[*1]ID codes (shown in brackets): Sigma-Aldrich (numerical and B8806), Fluka (ANIL01600), or Invitrogen (other alfanumerical).
[*2]Values actually used in the present study.
[*3]Manufacturers' data.
[*4]1P denotes one-photon excitation (CLSM); 2P denotes two-photon excitation (TPEM).

maintaining the best signal-to-noise ratio throughout the sample; (2) offline method—a custom plug-in for the *Ellipse* modular software package (ViDiTo, Slovakia; www.vidito.com), adjusting the brightness and contrast in an image series (stack) so that the effect of light attenuation is minimized (Čapek et al., 2006).

Autofluorescence was recorded at an excitation/detection wavelength of 633/650–710 nm.

Two-Photon Excitation Microscopy

An above-mentioned confocal microscope (Leica TCS SP2 AOBS) was used in concert with a Ti:Sapphire Chameleon Ultra family femtosecond laser Mira 900 (Coherent, Santa Clara, CA, USA) tunable from 690 to 1,040 nm. A two-photon fluorescence signal was collected by an internal detector placed in the scanning head of the confocal microscope (descanned, backscattering geometry). The detected wavelength was adjusted by applying lambda scans to maximize the fluorescence signal of the sample. The average laser power on the sample was in the order of milliwatts.

3D Visualization

CLSM and TPEM provided a series of perfectly aligned optical sections of TA cells. To visualize them as 3D objects, we used the *Ellipse* software package (ViDiTo Systems, Košice, Slovakia) adapted to work with a specialized Volume-Pro 1000 board (www.terarecon.com), performing volume rendering of digital scalar data in real time (Čapek et al., 2009).

Stereological Measurement

The biovolume inside TA shells was determined by the stereological "Fakir" method from images acquired by CLSM or TPEM (Cruz-Orive, 1997; Kubínová & Janáček, 2001; Kubínová et al., 2002). The fakir probe (Cruz-Orive, 1997) is a systematic probe consisting of parallel test lines (resembling nails of a fakir's bed and piercing its surface). We applied a highly efficient spatial grid consisting of three mutually perpendicular half-period shifted fakir probes (Kubínová & Janáček, 1998, 2001; Difato et al., 2004). The TA biovolume (V) was estimated by the following formula:

$$estV = \tfrac{1}{3} \cdot u^2 \cdot (L_1 + L_2 + L_3),$$

where L_i ($i = 1,2,3$) is the total length of object-to-probe intercepts (i'th fakir probe), the object being the biomass boundary; u is the grid constant, i.e., the smallest distance between neighboring parallel lines of the fakir probe. The position of the spatial grid was random (Weibel, 1979).

RESULTS

Basic Morphology

The testate amoeba architecture was visualized by employing complementary optical contrasting modalities such as phase contrast (Fig. 1b), polarization (Fig. 1c,e,g), and DIC Nomarski (Fig. 1d,f,h) microscopy in unstained cells/shells. The origin of the optically active objects highlighted in
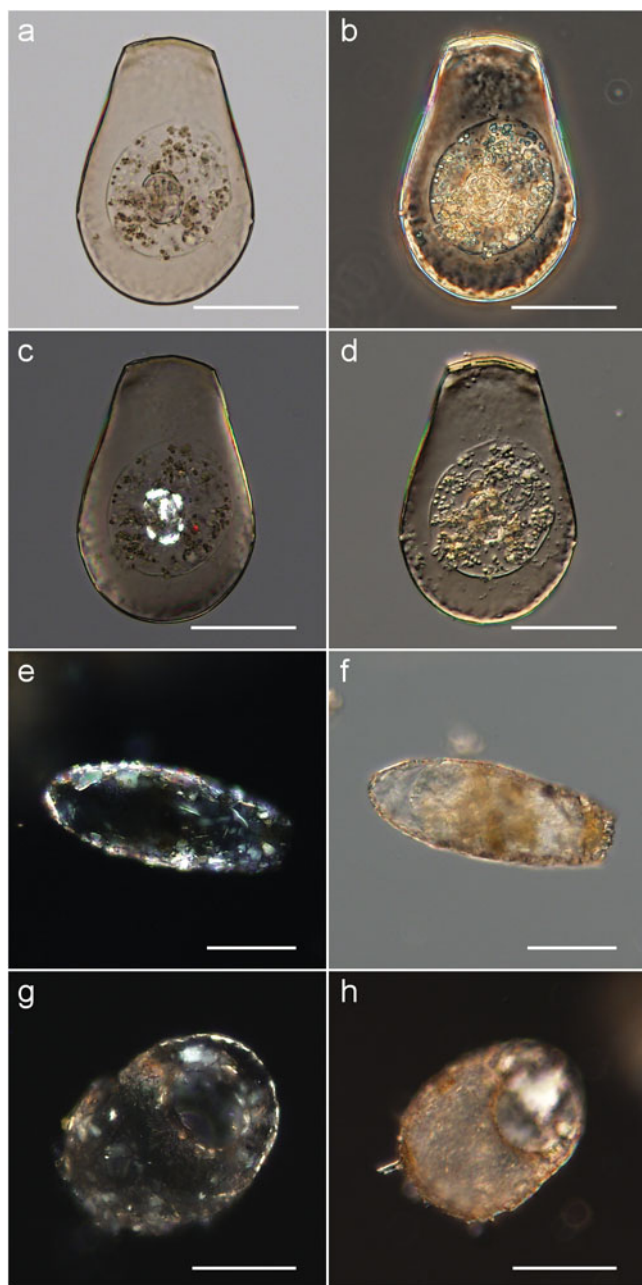
Surface Structures

SEM and ESEM were used to visualize the surface of TA shells at high resolution. It is possible to observe the shell coated with sand grains, its structure, and typical morphological characteristics (Fig. 2c,d,e).

As ESEM does not require the samples to be metal-coated, frequent artifacts caused by the coating procedure are eliminated. The only requirement is to avoid mechanical or chemical impurities, such as various particles or surface films. ESEM microscopy often yields better quality images of the shell, plus details just under the shell surface (Fig. 2e), in comparison to SEM. However, SEM or ESEM cannot be applied to visualize living TA.

Cellular Compartments

Labeling of the TA shell with acid fuchsin let us observe secreted scales, or organic or mineral xenosomes used as building blocks of the shell (Figs. 2a, 3m, 4a). In some cases, the SEM and CLSM images nicely complement each other (Fig. 2). Acid fuchsin also reveals the internal structure of the cell (Fig. 2a,b,f,g), and such data can be combined with autofluorescence observations of chlorophyll present in endosymbionts (Fig. 3a,b).

Fluorescein derivative BCECF-AM labeled the cytoplasm in living TA individuals only (Fig. 3c,e), including a protoplast, most likely of another organism, inside an otherwise empty shell (Fig. 4e) or even cell nuclei during mitosis (Fig. 4f). In living TA, BCECF-AM also stains the shell (Fig. 3e) and its architecture can be observed in great detail (Fig. 4c). However, the image is not as sharp as in the case of acid fuchsin. BCECF-AM can also be used to determine cytosolic pH (Fig. 4h).

Propidium iodide stains nucleic acids in dead individuals (Fig. 3h). $DiOC_3(3)$ stains membranes, including those of organelles within the cell (Fig. 3i,j). Mitochondria can be specifically labeled by MitoTracker Deep Red FM (Fig. 3k) and TMRE (Fig. 3l). Aniline blue visualizes some components of TA shells and appears to be complementary to acid fuchsin (Fig. 3m). CellTracker Green CMFDA also labels living TA (Fig. 3n). Er-Tracker Blue White DPX stains the endoplasmic reticulum of TA (Fig. 3o). FITC binds to proteins within the cell (Figs. 3p, 5a,b). The vacuoles of *Hyalosphenia papilio* labeled by FITC (Figs. 3f,p, 5a) were visualized using a single laser line wavelength (488 nm).

Staining by Hoechst 34580, DAPI, LysoTracker Red DND-99, AlexaFluor 633 phalloidin, SYTO 16, and Texas Red C_2-maleimide was unsuccessful (data not shown). Other results are summarized in Table 3.

Endosymbiotic Algae

Autofluorescence was recorded in *Archerella flavum* (Fig. 3a) and *Hyalosphenia papilio* (Figs. 3b,f,i,j,l,p, 4f). Both of them are mixotrophic species (i.e., TA containing endosymbiotic
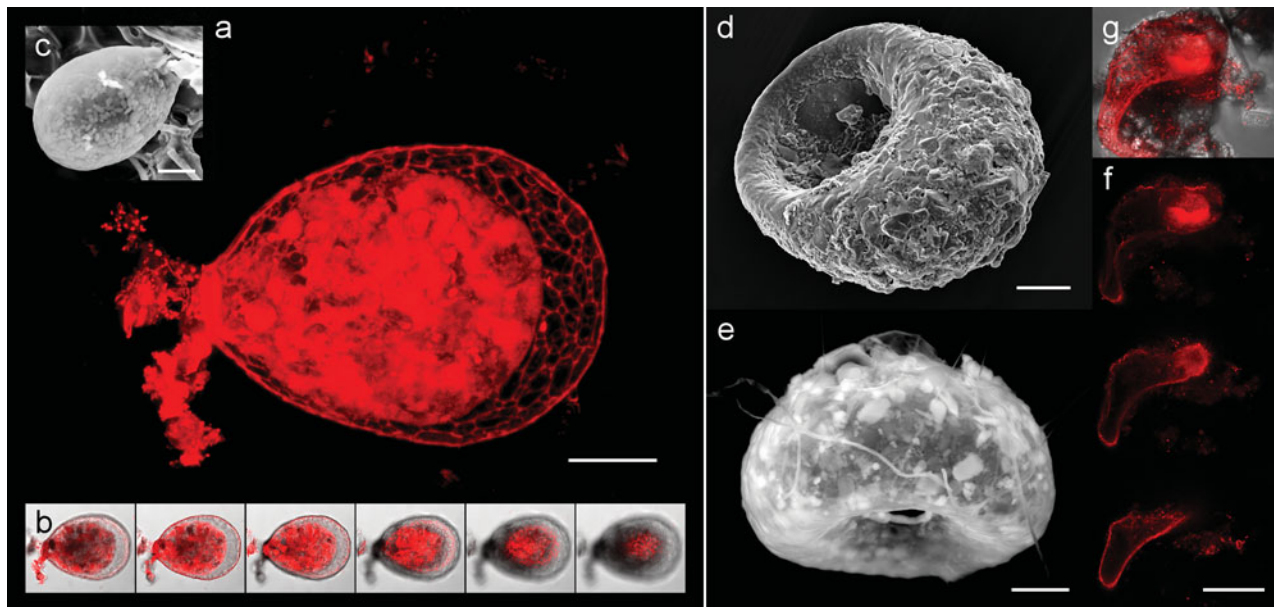

Figure 1. Optical contrasting of unstained testate amoebae: (**a–d**) *Hyalosphenia papilio* (cyst), (**e,f**) *Difflugia oblonga* (living cell), and (**g,h**) *Centropyxis sp.* (two similar but different cells). Note the complementary nature of (**a**) bright field, (**b**) phase contrast, (**c,e,g**) polarization, and (**d,f,h**) DIC Nomarski imaging. Scale bar in all images, 50 μm.

Figure 1c is unclear and requires further elucidation. Test scales and/or sand grains adsorbed on the test surface are also highlighted by polarization microscopy (Fig. 1e,g). The cyst architecture is best visualized by DIC Nomarski imaging (Fig. 1d) while its outline is better rendered by phase contrast (Fig. 1b). A bright-field image (no optical contrasting) is shown for comparison (Fig. 1a).

Figure 2. Shell (test) shapes and surface structures visualized by CLSM, SEM, and ESEM. **a,b:** *Nebela tincta* in CLSM (acid fuchsin staining); (**a**) maximum intensity projection, scale bar 20 μm, (**b**) serial optical sections (overlay with bright field). **c:** *Nebela tincta* in ESEM, scale bar 20 μm. **d:** *Centropyxis aculeata* in SEM, details of aperture, scale bar 20 μm. **e:** *Trigonopyxis arcula* in ESEM, scale bar 20 μm. **f,g:** *Centropyxis aculeata* in CLSM (acid fuchsin staining), cyst inside the test, scale bar 50 μm; (**f**) serial optical sections, (**g**) overlay of bright field and maximum intensity projection of image **f**.

algae with chlorophyll that exhibits autofluorescence). This phenomenon could be useful in studies of symbionts inside mixotrophic TA species. No autofluorescence was found in heterotrophic species.

Identification of Living and Dead Amoebae

A combination of BCECF-AM and propidium iodide fluorescent probes, commonly used to assess cell vitality (King,

2000), can be successfully applied to separate dead and living TA (Table 1). While propidium iodide stained nucleic acids in dead cells with permeable membrane (Fig. 3h), fluorescence of BCECF-AM could only be observed in living cells with an intact membrane (Fig. 3c,e), owing to enzymatic processes that activate the fluorescent probe (see Discussion for details). Amoebae shown in Fig. 3c,e,h were subjected to the combined two-probe staining.

Table 3. Suitability of Fluorescent Probes for Visualization of Various Compartments and Endosymbionts of Testate Amoebae (− Unsuccessful, + Poor, ++ Successful, +++ Excellent Labeling).

Fluorescent Probe	Targets of Fluorescent Probes					
	Nucleolus, Nucleus	Cytoplasm	Membranes	Shell	Specific Organelles	Symbionts
Acid Fuchsin	−	+++	−	+++	−	−
Aniline Blue	−	−	−	+	−	−
BCECF-AM	−	++	+	+	−	−
CellTracker Green CMFDA	−	+	−	−	+++ [*]	−
DiOC$_3$(3)	−	−	+++	+	−	−
Er-Tracker Blue-White DPX	−	−	−	−	++	−
FITC	−	+++	−	+	−	−
MitoTracker Deep Red FM	−	−	−	−	++	+++
Propidium Iodide	+	−	−	−	−	−
TMRE	−	−	−	−	+++	−

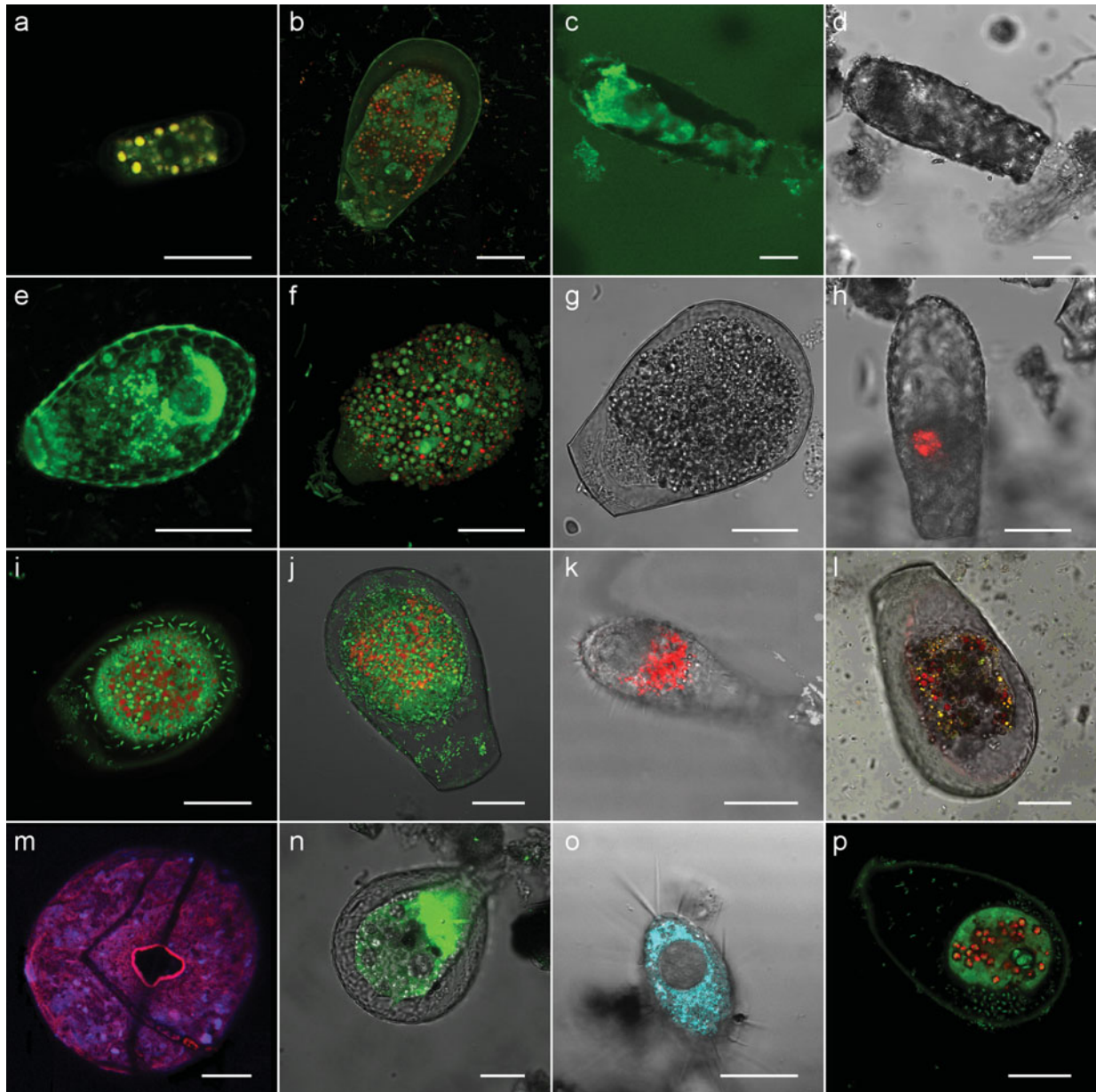[*]Organelles are visualized indirectly, owing to staining of the surrounding cytoplasm (Fig. 3n).

Figure 3. Testate amoebae in CLSM as stained by various fluorescent probes. **a:** *Archerella flavum*, cytoplasm and nucleolus (green, acid fuchsin) and endosymbionts' chlorophyll-a (red, autofluorescence), maximum intensity projection; yellow color is due to overlaying red and green channels. **b:** *Hyalosphenia papilio*, cytoplasm (green, acid fuchsin) and endosymbionts' chlorophyll (red, autofluorescence). **c:** *Difflugia oblonga*, cytoplasm of living TA (green, BCECF-AM). **d:** *Difflugia oblonga*, bright-field image of **c. e:** *Euglypha sp.*, cytoplasm and test (green, BCECF-AM), maximum intensity projection; uneven cytoplasm staining may be attributed to a varying esterase activity across cellular compartments. **f:** *Hyalosphenia papilio*, generic staining, preferentially of amine and sulfhydryl groups on protein molecules (green, FITC) and endosymbionts' chlorophyll (red, autofluorescence), maximum intensity projection. **g:** *Hyalosphenia papilio*, bright-field image of **f. h:** *Difflugia oblonga*, nucleus (nucleic acids) in dead TA (red, propidium iodide), overlay with bright field. **i,j:** *Hyalosphenia papilio*, membranes of living TA [green, DiOC$_3$(3)] and endosymbionts' chlorophyll (red, autofluorescence); (**j**) overlay of maximum intensity projection and bright field. **k:** *Euglypha sp.*, mitochondria (red, MitoTracker Deep Red FM), overlay of maximum intensity projection and bright field. **l:** *Hyalosphenia papilio*, mitochondria (yellow, TMRE), endosymbionts' chlorophyll (red, autofluorescence), overlay with bright field. **m:** *Trigonopyxis arcula*, test (blue, aniline blue; red, acid fuchsin), maximum intensity projection. **n:** *Nebela bohemica*, generic staining (green, CellTracker Green CMFDA), overlay with bright field. **o:** *Euglypha sp.*, endoplasmatic reticulum (cyan, Er-Tracker Blue-White DPX), overlay with bright field. **p:** *Hyalosphenia papilio*, cyst, generic staining (green, FITC) and endosymbionts' chlorophyll (red, autofluorescence). Scale bar in all images, 30 μm.
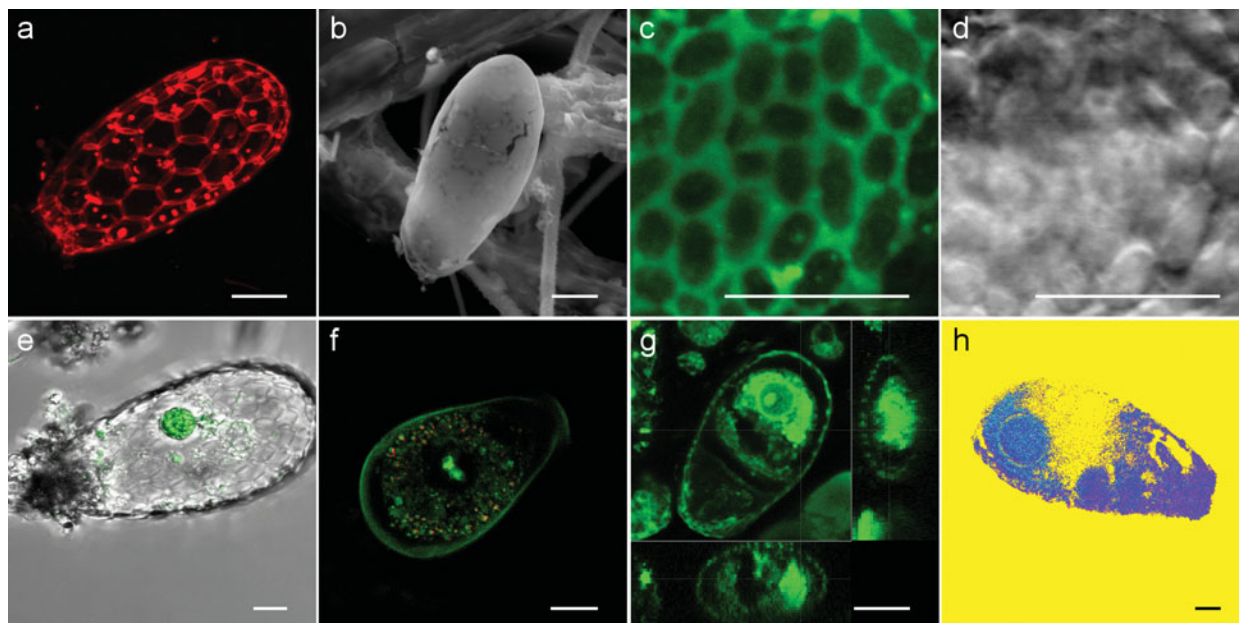
Figure 4. Advantages of CLSM imaging of testate amoebae. **a:** *Tracheleuglypha dentata* in CLSM, empty test (red, acid fuchsin), maximum intensity projection, scale bar 10 μm. **b:** *Trinema sp.* in ESEM, test surface, scale bar 10 μm. **c,d:** *Nebela bohemica* in CLSM, detail of the test structure (green, BCECF-AM); (**c**) maximum intensity projection, (**d**) bright field, scale bar 10 μm. **e:** *Euglypha sp.* in CLSM, protoplast inside the test (green, BCECF-AM), overlay with bright field, scale bar 10 μm. **f:** *Hyalosphenia papilio* in CLSM, cell nucleus in mitosis and cytoplasm (green, BCECF-AM) and endosymbionts' chlorophyll (red, autofluorescence), scale bar 30 μm. **g:** *Corythion dubium* in CLSM, cytoplasm and test (green, BCECF-AM) with lateral views (optical sections along the white lines are more visible in the online version), scale bar 10 μm. **h:** *Euglypha sp.*, pH distribution determined by BCECF-AM (ratiometric probe, pH-to-color not assigned, pseudocolor image), scale bar 10 μm.
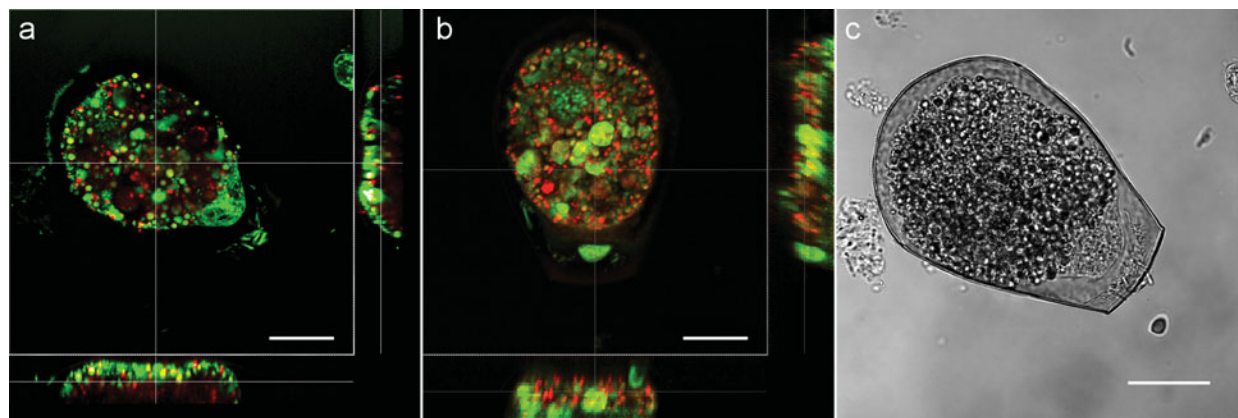

Figure 5. Comparison of CLSM and TPEM in terms of penetrating depth (shown in lateral views) in *Hyalosphenia papilio*. Organic components (green, FITC) and endosymbionts' chlorophyll (red, autofluorescence); (**a**) CLSM, (**b**) TPEM, and (**c**) bright-field image of **a**. Scale bar in all images, 30 μm.

Rose Bengal (rB) is also commonly used to identify dead and living TA individuals (Patterson et al., 2002). However, no living specimens were detected by rB in our samples from the same locality and time. This may be attributed to generic problems with rB staining as described by Bernhard (2000). Thus, we recommend the BCECF-AM + propidium iodide method over rB staining alone to identify dead/living TA individuals. Separating dead and living TA individuals is important in ecological studies (Nguyen-Viet et al., 2008). Moreover, propidium iodide also

Table 4. Biovolume of Testate Amoeba Inside Their Shells Evaluated by the Stereological Fakir Method.

Sample	Dye	Length (μm)	Width (μm)	Biovolume (μm^3)
Euglypha sp.	BCECF-AM	64.6	34.1	3.04×10^4
Cyphoderia ampulla	BCECF-AM	112	50.5	3.90×10^4
Difflugia oblonga	BCECF-AM	164	57.3	2.41×10^5
Euglypha sp. (cyst)	Acid fuchsin	53	25	9.74×10^3

allows counting of nuclei, which is important in taxonomy (Meisterfeld, 2002*a*, 2002*b*).

Opaque/Large Amoebae

In small TA species (10–100 μm) with translucent shells, standard CLSM yields satisfactory results (Fig. 4g). Problems occur with larger (thicker) species and those that build opaque shells (typically made of agglutinated organic or mineral particles). Since both emission and excitation light is strongly absorbed by the shell and the amoeba itself, CLSM typically makes it possible to acquire TA images from depths up to 20 μm only (Fig. 5a). In deeper layers the images suffer from low signal-to-noise ratio.

These problems are partly solved by TPEM whose excitation light is in the infrared range capable of penetrating deeper into most biological objects (Fig. 5b), up to 70 μm in TA. This is sufficient for the vast majority of TA species and enables biovolume estimation of the amoeba inside the shell, and 3D reconstructions.

3D and Biovolume Data

3D visualizations based on CLSM and TPEM images (acquired from one direction only) make it possible to examine the object from any angle (Fig. 6). Owing to the 3D data, it is possible to precisely localize in the amoeba chlorophyll (Fig. 6a–d), the activity of nonspecific esterases (Fig. 6e–h) or any other fluorescent structure of interest.

The results of stereological biovolume measurement in four TA specimens are summarized in Table 4. By using the "Fakir" method, we were able to evaluate biovolumes with sufficient accuracy while keeping the image acquisition time reasonably short (tens of minutes per one image stack).

Discussion

Future progress in testate amoeba taxonomy and ecology requires a detailed morphological characterization of their shells and cells, as it helps to select the criteria for distinguishing closely related, morphologically similar species. A detailed examination of cell content, e.g., quantification of organelles and (in mixotrophic species) endosymbionts, or biovolume estimation yields information about the physiological state of the amoeba, with implications in ecophysiology and ecotoxicology. Likewise, it is important to reliably recognize living and dead individuals.

The relatively simple optical contrasting modalities such as phase contrast, DIC-Nomarski, or Hoffman modulation contrast reveal the variations of a refractive index within the specimen and are akin to the digital holographic microscopy mentioned toward the end of Discussion. They are particularly suitable for examining nonabsorbing objects such as unstained living cells (Murphy, 2001). The structure of the TA shell can often be visualized by a simple polarization microscopy at a negligible cost, owing to the shell's (bio)mineralized nature (Fig. 1e,g). In this context, such modes are complementary with CLSM better capable of visualizing cell components stained with specific fluorescent probes. For example, BCECF-AM binds to the organic part of the TA shell only (Fig. 4c).

SEM and ESEM are frequently used for taxonomical descriptions of testate amoebae, and less often in ecological studies. They make it possible to examine the surface features of TA at high resolution and a very reasonable depth of field, and to perform quantitative elemental analyses of shell structures (Ogden & Hedley, 1980; Todorov et al., 2009). However, SEM and ESEM cannot be used to examine living TA or the inner architecture of the amoeba or the shell. Conventional SEM can only operate in a high-vacuum mode, which dictates the rather complex specimen preparation protocol, itself a source of a number of artifacts. ESEM and some of its alternatives, such as variable pressure SEM (VP-SEM), allow the examination of specimens under a wide range of gaseous conditions. These permit an investigation of the biological samples, usually only nonliving ones, in a closer-to-natural (uncoated) state, and are applicable to practically any TA shell type. The drawback is a lower image contrast of the uncoated sample.

The fluorescent probes required in CLSM can penetrate into the amoeba only through the shell operculum and some of them thus require a longer loading/staining time. The reproducibility of the labeling protocols is often problematic. For example, *Acanthamoeba castellanii* was successfully labeled by rhodamine tagged phalloidin complex to visualize actin (González-Robles et al., 2008). However, we failed to stain TA with this probe.

It is more difficult to stain shell-enclosed TA than naked amoebae or animal cells. The same applies to foraminifera that also build their shells with an operculum. Bernhard et al. (2004) successfully stained foraminifera by calcein, which we have not tested in TA. Instead, we experimented with fluorescein derivative BCECF-AM, a similar type of fluorescent probe. In many cases a trial-and-error approach had to be applied to optimize the labeling protocols in terms of photodamage, toxicity, and photobleaching, and ten fluorescent probes were successfully used.
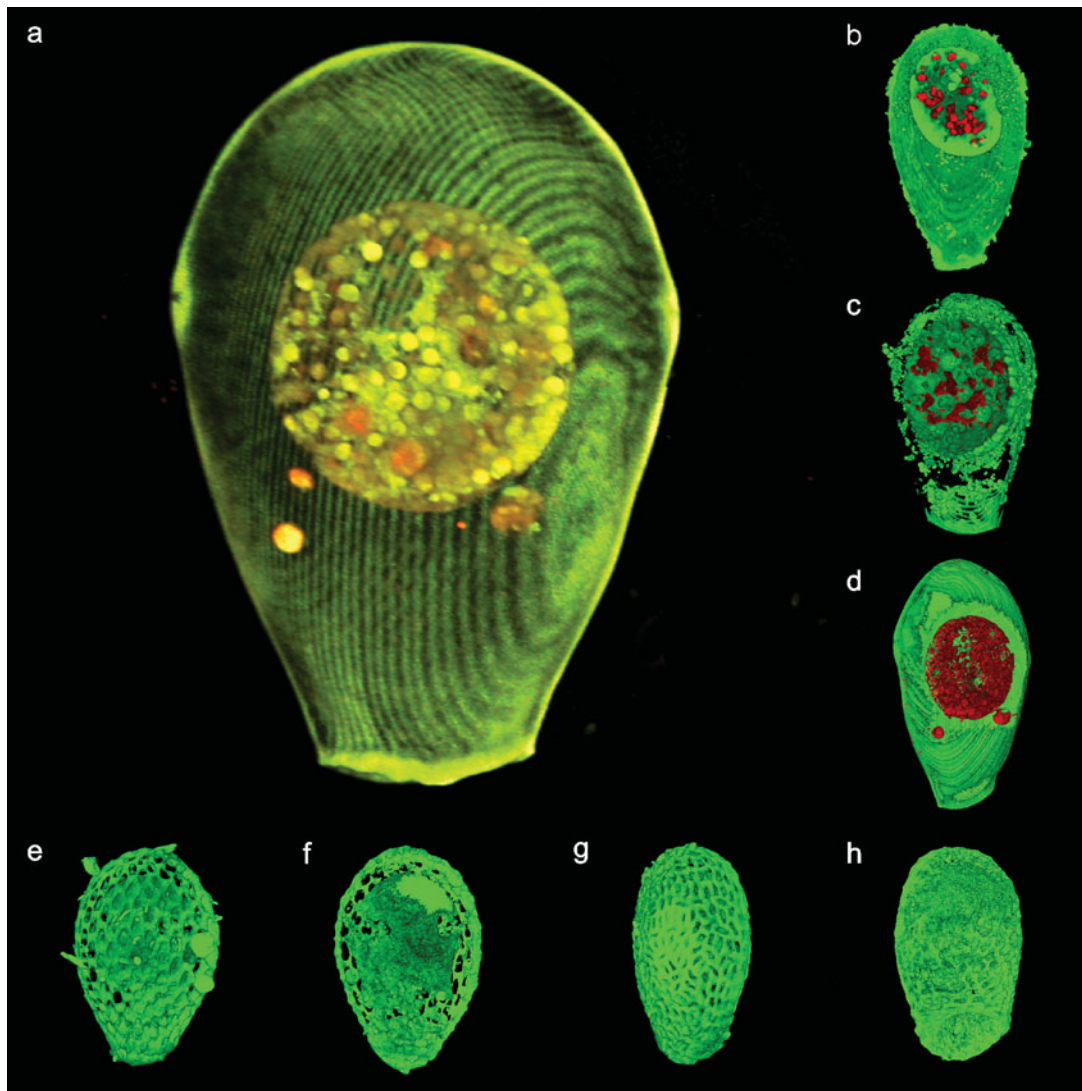
Figure 6. 3D reconstructions of testate amoebae. **a–d:** *Hyalosphenia papilio* test (ca. 150 μm in length), membranes and shells [green, DiOC$_3$(3)] and endosymbionts' chlorophyll (red, autofluorescence) in CLSM (the surface layer lines represent the amoebae outline in individual optical sections used in the reconstructions); (**a**) VolumePro 1000 rendering board, (**b–d**) OpenGL-based volume rendering; the same cell is shown in images **a** and **d**. **e,f:** *Euglypha sp.* test (75 μm in length, original image in Fig. 3e), shells and enzymatic activity of cytoplasm (green, BCECF-AM) in CLSM, maximum intensity projection; (**e**) front view, (**f**) rear view. **g,h:** *Corythion dubium* test (35 μm in length, original image in Fig. 4g), shells and enzymatic activity in cytoplasm (green, BCECF-AM) in CLSM, maximum intensity projection; (**g**) front view, (**h**) rear view.

Rose Bengal (rB) is the most commonly used probe to distinguish live/dead shell-enclosed TA or foraminifera cells. rB is a biological dye that is supposed to bind to cytosolic proteins, rendering the cytoplasm in a rose color (Walton, 1952). The main advantages of rB are quick staining and a relatively low price. However, necrotic as well as healthy cytoplasm is stained in foraminifera. It has been shown that rB reacts even weeks or months after individual's death. Moreover, even specimens known to contain dead cells do not always become rB stained (Martin & Steinker, 1973; Lutze & Altenbach, 1991). Generally, rB

should not be used as the only dye to detect live/dead cells (Bernhard, 2000). Sudan black (a lipophilic stain) is yet another probe that is often used to distinguish live/dead foraminifera and suffers from similar drawbacks as rB—staining opaque specimens may yield ambiguous results (Bernhard, 2000).

These problems are absent if a combination of BCECF-AM and propidium iodide is used; live/dead TA are clearly distinguished. BCECF-AM probe is nonfluorescent and membrane-permeable in its basic state. Upon cleavage by nonspecific esterases, it becomes fluorescent but also mem-

brane impermeable, so it gets trapped in living cells but quickly disappears from dead or membrane-damaged cells. Surprisingly, we observed fluorescence not only inside the living cells, but also in the shells of living amoebae (between idiosomes), perhaps due to nonspecific esterases that may be part of the organic (proteinaceous) matrix sustaining the shell. This notion is supported by the fact that the fluorescence was detected in the shells of living TA only.

In mammalian tissues, mitochondria are among the first organelles that exhibit distinct structural alterations during necrosis (Raffray & Cohen, 1997). If intact mitochondria are observed in TA, one may conclude that the cell is alive at the time of staining. In our samples differences were encountered in spatial distribution of mitochondria between *Euglypha sp.* (a heterotrophic species) labeled by MitoTracker Deep Red FM (Fig. 3k) and *Hyalosphenia papilio* (a mixotrophic species) labeled by TMRE (Fig. 3l). It is premature yet to draw any conclusions about the two nutrition strategies but both of these probes are known to accumulate in active mitochondria only.

To determine the biomass inside the shell, an optical diffraction tomography technique based on digital holographic microscopy (DHM) can be utilized. This method, essentially an adaptation of an interference-phase microscopy utilizing coherent light, enables a tomographic reconstruction of the microscopic object with a resolution of ca. 1.5 μm in all three directions (Charrière et al., 2006). Very small objects such as organelles or endosymbionts are better modeled by CLSM owing to its optical sectioning capability and better lateral/axial resolution (Diaspro, 2002; Matsumoto, 2002; Pawley, 2006) although in larger specimens such as *Hyalosphenia papilio*, the laser light cannot penetrate sufficiently deep into the amoeba, and TPEM (Denk et al., 1990; Diaspro, 2002) would have to be employed instead. In DHM, this problem is mitigated simply by rotating the sample.

Nguyen-Viet et al. (2008) evaluated TA biovolumes by assuming they are of regular geometrical shapes. Obviously, this methodology enables fast volume measurements at the expense of accuracy.

Conclusion

The present study highlights the advantages and limitations of various specialized microscopic imaging modalities, as applied to testate amoeba morphology. The CLSM and TPEM data are the first of its kind obtained in testate amoebae. Jointly with associated 3D reconstructions and stereological analyses, the multimodal imaging is of potential interest, e.g., in taxonomy, ecophysiology, or ecotoxicology.

Acknowledgments

References

Aoki, Y., Hoshino, M. & Matsubara, T. (2007). Silica and testate amoebae in a soil under pine-oak forest. *Geoderma* **142**, 29–35.

Bernhard, J.M. (2000). Distinguishing live from dead foraminifera: Methods review and proper applications. *Micropaleontology* **46**(S1), 38–46.

Bernhard, J.M., Blanks, J.K., Hintz, Ch.J. & Chandler, G.T. (2004). Use of the fluorescent calcite marker calcein to label foraminiferal tests. *J Foraminiferal Res* **34**, 96–101.

Beyens, L. & Meisterfeld, R. (2001). Protozoa: Testate amoebae. In *Tracking Environmental Change Using Lake Sediments: Volume 3: Terrestrial, Algal, and Siliceous Indicators*, Smol, J.P., Birks, H.J.B. & Last, W.M. (Eds.), pp. 121–153. Dordrecht, Netherlands: Kluwer Academic Publishers.

Booth, R.K. (2002). Testate amoebae as paleoindicators of surface-moisture changes on Michigan peatlands: Modern ecology and hydrological calibration. *J Paleolimn* **28**, 329–348.

Čapek, M., Brůža, P., Janáček, J., Karen, P., Kubínová, L. & Vágnerová, R. (2009). Volume reconstruction of large tissue specimens from serial physical sections using confocal microscopy and correction of cutting deformations by elastic registration. *Microsc Res Tech* **72**, 110–119.

Čapek, M., Janáček, J. & Kubínová, L. (2006). Methods for compensation of the light attenuation with depth of images captured by a confocal microscope. *Microsc Res Tech* **69**, 624–635.

Charrière, F., Pavillon, N., Colomb, T., Depeursinge, Ch., Heger, T.J., Mitchell, E.A.D, Marquet, P. & Rappaz, B. (2006). Living specimen tomography by digital holographic microscopy: Morfometry of testate amoeba. *Opt Express* **14**, 7005–7013.

Cruz-Orive, L.M. (1997). Stereology of single objects. *J Microsc (Oxford, U.K.)* **186**, 93–107.

Denk, W., Strickler, J.H. & Webb, W.W. (1990). Two-photon laser scanning fluorescence microscopy. *Science* **248**, 73–76.

Diaspro, A. (2002). *Confocal and Two-Photon Microscopy: Foundations, Applications, and Advances*. New York: Wiley-Liss.

Difato, F., Mazzone, F., Scaglione, S., Fato, M., Beltrame, F., Kubínová, L., Janáček, J., Ramoino, P., Vicidomini, G. & Diaspro, A. (2004). Improvement in volume estimation from confocal sections after image deconvolution. *Microsc Res Tech* **64**, 151–155.

Foissner, W. (1997). Protozoa as bioindicators in agroecosystems, with emphasis on farming practices, biocides, and biodiversity. *Agric Ecosyst Environ* **62**, 93–103.

Foissner, W. (1999). Soil protozoa as bioindicators: Pros and cons, methods, diversity, representative examples. *Agric Ecosyst Environ* **74**, 95–112.

Gilbert, D., Amblard, C., Boudier, G. & Frances, A.J. (1998). The microbial loop at the surface of a peatland: Structure, function and impact of nutrient input. *Microb Ecol* **35**, 83–93.

González-Robles, A., Castañón, G., Hernández-Ramírez, V.I., Salazar-Villatoro, L., González-Lázaro, M., Omaña-Molina, M., Talamás-Rohana, P. & Martínez-Palomo, A. (2008). *Acanthamoeba castellanii*: Identification and distribution of actin cytoskeleton. *Exp Parasitol* **119**, 411–417.

Heger, T.J., Mitchell, E.A.D., Todorov, M., Golemansky, V., Lara, E. & Pawlowski, J. (2010). Molecular phylogeny of euglyphid testate amoebae (Cercozoa: Euglyphida) suggest transitions between marine supralittoral and freshwater/terrestrial environments are infrequent. *Mol Phylogenet Evol* **55**, 113–122.

King, M.A. (2000). Detection of dead cells and measurement of cell killing by flow cytometry. *J Immunol Methods* **234**, 155–166.

Kubínová, L. & Janáček, J. (1998). Estimating surface area by the isotropic fakir method from thick slices cut in an arbitrary direction. *J Microsc (Oxford, U.K.)* **191**, 201–211.

Kubínová, L. & Janáček, J. (2001). Confocal microscopy and stereology: Estimating volume, number, surface area and length by virtual test probes applied to three-dimensional images. *Microsc Res Tech* **53**, 425–435.

Kubínová, L., Janáček, J. & Krekule, I. (2002). Stereological methods for estimating geometrical parameters of microscopic structure by three dimensional imaging. In *Confocal and Two Photon Microscopy: Foundations, Applications, and Advances*, Diaspro, A. (Ed.), pp. 299–332. New York: Wiley-Liss.

Lutze, G.F. & Altenbach, A.V. (1991). Technik und Signifikanz der Lebenfärbung der benthischer Foraminiferen mit Bengalrot. *Geol Jahr* **A128**, 251–265 (with English abstract).

Madrid, R.E. & Felice, C.J. (2005). Microbial biomass estimation. *Crit Rev Biotechnol* **25**, 97–112.

Martin, R.E. & Steinker, D.C. (1973). Evaluation of techniques for recognition of living foraminifera. *Compass Sigma Gamma Epsilon* **50**, 26–30.

Matsumoto, B. (2002). *Cell Biological Applications of Confocal Microscopy*. San Diego, CA: Academic Press.

Meisterfeld, R. (2002a). Order Arcellinida Kent, 1880. In *An Illustrated Guide to the Protozoa*, 2nd ed., Lee, J.J., Leedale, G.F. & Bradbury, P. (Eds.), vol. 2, pp. 827–860. Lawrence, KS: Society of Protozoologists.

Meisterfeld, R. (2002b). Testate amoebae with filopodia. In *An Illustrated Guide to the Protozoa*, 2nd ed., Lee, J.J., Leedale, G.F. & Bradbury, P. (Eds.), vol. 2, pp. 1054–1084. Lawrence, KS: Society of Protozoologists.

Michels, J. & Schnack-Schiel, S.B. (2005). Feeding in dominant Antarctic copepods—Does the morphology of the mandibular gnathobases relate to diet? *Mar Biol (Heidelberg, Ger.)* **146**, 483–495.

Mitchell, E.A.D., Charman, D.J. & Warner, B.G. (2008a). Testate amoebae analysis in ecological and paleoecological studies of wetlands: Past, present and future. *Biodiver Conserv* **17**, 2115–2137.

Mitchell, E.A.D. & Gilbert, D. (2010). Present status of testate amoeba research, knowledge gaps and research priorities. *Meeting Report: 5th International Symposium on Testate Amoebae (ISTA-5)*, Montbéliard, France, September 14–17, 2009. *Protist* **161**, 337–341.

Mitchell, E.A.D., Gilbert, D., Buttler, A., Amblard, C., Grosvernier, P. & Gobat, J.M. (2003). Structure of microbial communities in *Sphagnum* peatlands and effect of atmospheric carbon dioxide enrichment. *Microb Ecol* **46**, 187–199.

Mitchell, E.A.D., Payne, R.J. & Lamentowicz, M. (2008b). Potential implications of differential preservation of testate amoeba shells for paleoenvironmental reconstruction in peatlands. *J Paleolimn* **40**, 603–618.

Murphy, D.B. (2001). *Fundamentals of Light Microscopy and Electronic Imaging*. New-York: Wiley-Liss.

Nguyen-Viet, H., Bernard, N., Mitchell, E.A.D., Badot, P.M. & Gilbert, D. (2008). Effect of lead pollution on testate amoebae communities living in *Sphagnum fallax*: An experimental study. *Ecotoxicol Environ Safe* **69**, 130–138.

Ogden, C.G. & Hedley, R.H. (1980). *An Atlas of Freshwater Testate Amoebae*. New-York: Oxford University Press.

Patterson, R.T., Barker, T. & Burbidge, S.M. (1996). Arcellaceans (thecamoebians) as proxies of arsenic and mercury contamination in northeastern Ontario lakes. *J Foraminiferal Res* **26**, 172–183.

Patterson, R.T., Dalby, A., Kumar, A., Henderson, L.A. & Boudreau, R.E.A. (2002). Arcellaceans (thecamoebians) as indicators of land-use change: Settlement history of the Swan Lake area, Ontario as a case study. *J Paleolimn* **28**, 297–316.

Pawley, J.B. (2006). *Handbook of Biological Confocal Microscopy*. New York: Springer.

Raffray, M. & Cohen, G.M. (1997). Apoptosis and necrosis in toxicology: A continuum or district modes of cell death? *Pharmacol Ther* **75**, 153–177.

Schönborn, W. (1983). Relationships between production, mortality and abundance in Testacean (Protozoa) communities in soil. *Pedobiologia* **25**, 403–412.

Schönborn, W. (1992). The role of protozoan communities in freshwater and soil ecosystems. *Acta Protozool* **31**, 11–18.

Schröter, D., Wolters, V. & De Ruiter, P.C. (2003). C and N mineralisation in the decomposer food webs of a European forest transect. *Oikos* **102**, 294–308.

Todorov, M., Golemanski, V., Mitchell, E.A.D. & Heger, T.J. (2009). Morphology, biometry, and taxonomy of freshwater and marine interstitial Cyphoderia (Cercozoa: Euglyphida). *J Eukaryotic Microbiol* **56**, 279–289.

Vohník, M., Burdíková, Z., Albrechtová, J. & Vosátka, M. (2009). Testate amoebae (Arcellinida and Euglyphida) vs. ericoid mycorrhizal and DSE fungi: A possible novel interaction in the mycorrhizosphere of Ericaceous plants? *Microb Ecol* **57**, 203–214.

Walton, W.R. (1952). Techniques for recognition of living foraminifera. *Contributions from the Cushman Foundation for Foraminiferal Research* **3**, 56–60.

Wanner, M. (1999). A review on the variability of testate amoebae: Methodological approaches, environmental influences and taxonomical implications. *Acta Protozool* **38**, 15–29.

Weibel, E.R. (1979). *Stereological Methods, Vol. 1: Practical Methods for Biological Morphometry*. London: Academic Press.

Wilkinson, D.M. (2008). Testate amoebae and nutrient cycling: Peering into the black box of soil ecology. *Trends Ecol Evol* **23**, 596–599.